International Forum on Aeroelasticity and Structural Dynamics
IFASD 2017
25-28 June 2017, Como - Italy

AEROSERVOELASTIC STABILITY ANALYSIS USING RESPONSE-BASED PARAMETRIC FLUTTER MARGINS

Federico Roizner[1] and Moti Karpel[1]

[1] Faculty of Aerospace Engineering
Technion – Israel Institute of Technology
froizner@campus.technion.ac.il

Keywords: Flutter, LCO, aeroservoelasticity

Abstract: A new parametric flutter margin method for linear and nonlinear stability analysis of aeroservoelastic systems is presented. The method is based on frequency response calculations with the system stabilized using a single parameter, which facilitates convenient response calculations with smooth response variations with respect to excitation frequency and air velocity. The frequency response functions are used for generating flutter margins with respect to the added parameter. The linear flutter or nonlinear limit-cycle-oscillation conditions are those at which the margins are zero. The nonlinear process starts with a linear one, to which nonlinear effects are added using a non-iterative first-order harmonic-balance procedure. Two numerical examples, based on a generic transport aircraft model, are given: a linear one with a simple gust-alleviation control system, and a nonlinear one with control-surface actuator free play. The results demonstrate excellent agreement with those obtained using traditional flutter methods and nonlinear time-marching simulations.

1 INTRODUCTION

Flutter is a dynamic aeroservoelastic (ASE) instability phenomenon due to the interaction between aircraft structural dynamics, unsteady aerodynamic forces and flight control systems. Flutter conditions of a certain structural configuration are characterized by the flight parameters at which the system becomes unstable, the associated vibration frequency, and the flutter mode. At the flutter boundary, linear ASE systems exhibit harmonic oscillations in response to an initial excitation. Beyond the boundary, the vibration amplitude increases exponentially. Flutter of nonlinear systems may be defined similarly when small vibration amplitudes are assumed. However, when amplitudes grow, the nonlinear dependency on the amplitude may yield periodic motion, called limit-cycle oscillation (LCO) at pre- or post-flutter conditions without necessarily leading to damaging vibration levels.

At flutter onset conditions, an aircraft undergoes self-excited harmonic oscillations in response to any initial trigger. Accordingly, the frequency-domain (FD) linear ASE equation is homogenous, and can be written as follows

$$[A(i\omega)]\{x(i\omega)\} = \{0\} \tag{1}$$

where the closed-loop system matrix $[A(i\omega)]$ contains the generalized mass, damping, stiffness and frequency-depended aerodynamic matrices, and the control-system matrices (if any) that reflect the respective sensors, control laws and actuators; $\{x(i\omega)\}$ is the state vector containing the modal displacement vector and control states. Equation (1) has a non-trivial

solution if and only if $|A(i\omega)| = 0$. Consequently, common flutter methods concentrate on finding the conditions at which the ASE matrix determinant is zero, e.g. [1,2] for aeroelastic systems and [3,4] for ASE ones. The main difficulty stems from the fact that the aerodynamic force coefficient matrix and control laws depend on the resulting flutter frequency.

While being well established and widely used, the applicability of the common industrial flutter analysis methods is limited. Their main disadvantages are: (a) Requires dedicated flutter solvers such as *p*, *p-k* and *g*- method solvers. (b) Being based on the system matrix properties rather than response simulations, they are difficult to compare with wind-tunnel and flight tests results. (c) The solution reflects an actual physical situation only at the flutter point because it consists of adding an artificial term that is canceled only at this point. (d) It is difficult to obtain flutter margins with respect to design parameters that may be needed in the preliminary design stages. (e) The ASE matrix is singular at the flutter point, which makes it difficult to obtain time-domain (TD) solutions at the vicinity of this point; and (f) Cannot be extended directly to the investigation of nonlinear effects.

An existing way to overcome these disadvantages is by generating a state-space TD model using rational-function approximation [5,6] of the generalized force coefficient matrix. Then, TD simulations are performed by integrating the state-space equation where nonlinear effects can be easily added, e.g. [7,8]. Although this approach is often used in research, it is rarely used in industrial environment because it lacks the required level of efficiency, robustness and accuracy when applied to realistic models. A different approach to perform time-marching simulations, with no need of rational-function approximations, is the recently developed Increased-Order Modelling (IOM) approach [9] and the associated Dynresp framework code [10], where an ASE system is modeled as a linear block, augmented by feedback loops that reflect structural, aerodynamic, control and mechanical nonlinearities.

Theoretically, the LCO characteristics of a nonlinear ASE system can be obtained by analyzing the steady-state response of a time-marching simulation. However, this approach does not seem to be an appropriate method to perform a comprehensive industrial study of nonlinear ASE stability as the typically large model preparation and computation time limit the analyzed cases to a small number of aircraft configurations and flight conditions.

More efficient techniques to find LCO characteristics are the Describing Function and Harmonic Balance (HB) methods. The Describing Function technique (e.g. [11]) consists of finding an equivalent linear expression of the nonlinearity and performing a linear flutter analysis afterwards. This approach needs analytical or numerical work to find the equivalent linear coefficients, and seems to be difficult to apply to a system with more than one nonlinear element. For example, to find the LCO conditions with multiple nonlinearities [12] proposed to solve a nonlinear system of equations, instead of using the common flutter methods with the equivalent linear coefficients. The HB approach (e.g. [13-15]) assumes that the displacements, and the associated nonlinear forces, can be written as a Fourier series. LCO conditions are found when the Fourier summation expressions associated with each participating frequency are zero. The fundamental frequency is also unknown, and consequently two nonlinear coupled matrix equations must be solved simultaneously, one due to the nonlinear elements and the other one due to the nonlinear dependency on the frequency.

From this brief introduction, it is noted that linear and nonlinear ASE stability analyses are performed using different techniques. The typically gradual physical transition from linear to nonlinear flutter calls for using similar methodologies and disciplinary models for analyzing

both cases. This would simplify the combined flutter analysis, improve the physical insight and yield better understanding of the nonlinear effects. Therefore, an adequately accurate and robust stability analysis method which can be efficiently applied to both systems, linear and nonlinear, is desired.

A new response-based flutter analysis method that is applicable to both linear and nonlinear ASE systems is presented in this paper. It consists of introducing a stabilizing parameter, P_f, which alleviates the numerical difficulties near the stability boundaries of the original system. Then, by response analysis to harmonic excitations, flutter/LCO is found at the conditions at which the excitation and the stabilizing effects cancel each other. The key point is that, while the analyzed system is stable, the response mode obtained at this point is the same as the self-excited oscillations of the unmodified system. Furthermore, at flight conditions where the excitation does not cancel the stabilizing effects, flutter margins with respect to P_f can be found by using an expansion to the Nyquist gain-margin approach for single-input-single-output (SISO) systems [16]. Hence, the new method is called "Parametric Flutter Margin" (PFM). It was recently added to version 11 of the Dynresp code [10], with which the numerical applications of this paper were performed.

The paper is organized as follows: In Sec. 2 the mathematical formulation of the PFM method is presented. Section 3 presents the numerical examples comparing the PFM results to those calculating using standard commercial codes. Finally, concluding remarks are given in Sec. 4.

2 PARAMETRIC FLUTTER MARGIN METHOD

This section is divided into three subsections. In the first, we describe the new PFM method applied to linear systems for calculating their flutter characteristics. The second subsection expands the method for nonlinear LCO analyses, and the last one discusses some general implementation issues.

2.1 Linear PFM

In contrast to common flutter methods, the PFM procedure searches for the flutter boundary using frequency-response functions (FRFs) due to excitation introduced in the right-hand side of Eq. (1). Since dealing with FRFs is numerically difficult near the stability boundary due to the matrix singularity which causes the response to approach infinity, they are calculated with $[A(i\omega)]$ modified to include the effect of a stabilizing parameter P_f. The only constraint on P_f is that its effect can be removed by closing a SISO feedback loop. Even though the formulation below relates to the feedback loop as a control component, it can reflect any ASE parameter, as explained and demonstrated below. The open-loop modified equation of motion with the added parameter becomes

$$[A(i\omega)+P_f\{B_f\}\lfloor C_f(i\omega)\rfloor]\{x(i\omega)\} = \{B_f\}u_f(i\omega) \tag{2a}$$

$$y_f(i\omega) = \lfloor C_f(i\omega)\rfloor\{x(i\omega)\} \tag{2b}$$

where u_f and y_f are scalars, input and output of the modified system, and $\{B_f\}$ and $\lfloor C_f(i\omega)\rfloor$ are the respective distribution vectors. For any given $u_f(i\omega)$ Eq. (2) can be solved for $\{x(i\omega)\}$ and $y_f(i\omega)$ at all stable flight points, including the nominal flutter point that is now stable. The flight conditions and excitation frequency for which the resulting complex $y_f(i\omega)$ and the $u_f(i\omega)$ are related by

$$u_f(i\omega) = P_f y_f(i\omega) \tag{3}$$

must reflect flutter-onset conditions with $\omega=\omega_f$ being the flutter frequency. This can be easily proved by substituting Eq. (3) in Eq. (2), which eliminates both the added $P_f\{B_f\}[C_f(i\omega_f)]$ term in the system matrix and the right-side excitation term. Thus, Eq. (2) becomes the homogenous Eq. (1) to which the resulting $\{x(i\omega)\}=\{x_f(i\omega)\}$ is a nontrivial solution, namely the flutter mode.

To find the conditions at which Eq. (3) is satisfied, FRFs are first calculated at various flight conditions along a line in the flight envelope, such as a line of constant altitude or a line of constant Mach number. The FRF at each calculation point is then expressed by Bode plots of gain and phase variations with ω,

$$G(\omega) = 20\log_{10}|P_f y_f(i\omega) / u_f(i\omega)| \text{ [dB]} \tag{4a}$$
$$\Phi(\omega) = \angle P_f y_f(i\omega) / u_f(i\omega) \text{ [deg]} \tag{4b}$$

If the system is linear, the Bode plots can be generated with $u_f(i\omega)=(1.,0.)$. Phase-cross-over frequencies ω_{pco} are defined as those at which

$$\Phi(\omega_{pco}) = 360n, \qquad n = 0, \pm1, \pm2, \ldots \tag{5a}$$

that implies that $u_f(i\omega_{pco})$ and $y_f(i\omega_{pco})$ have the same phase. Even though we may be looking for a certain flutter mechanism, there may be no phase-cross-over frequencies, or more than one, in the searched frequency range. The parametric flutter margins are defined by the gain at each ω_{pco},

$$PFM = -G(\omega_{pco}) \tag{5b}$$

The repetition of the FRF calculations for various points along the selected flight-condition line yields the flutter conditions at which PFM=0[dB], which implies that Eq. (3) is satisfied. If, as often done, the flight-condition line is of various true velocities at a constant altitude, the interpolated point at which PFM=0[dB] is the flutter velocity V_f. The flutter frequency, ω_f, and mode, $\{x_f(i\omega_f)\}$, are the respective ω_{pco} and $\{x_f(i\omega_{pco})\}$ interpolated at V_f.

2.2 Nonlinear PFM

The frequency response approach to flutter analysis can still be applied when the system includes nonlinear elements. However, instead of looking for linear flutter where the response diverges to infinity, the search is now for a periodic self-excited response with limited amplitude, namely LCO. When the amplitude is large enough to cause substantial damage, there is no much difference between flutter and LCO. However, it is often small enough to be tolerated or even ignored.

The nonlinear effects depend on the excitation frequency and amplitude, and might result in LCOs with higher harmonics. It is assumed that the fundamental frequency of the return open-loop signal is the excitation one, as demonstrated in the numerical example. In this work, we focus on LCO analyses in which the nonlinearities can be represented by a single SISO nonlinear block, e.g. control-surface free play. Accordingly, a first-order non-iterative method is developed based on defining the nonlinear block as a part of the feedback loop that

remains open in the FD analysis, which was found to improve the computational time significantly. Higher-order iterative PFM methods were presented in Ref. [17].

The nonlinear effects are introduced by modifying the stability-boundary condition of Eq. (3) as follows

$$u_f(i\omega_f) = P_f y_f(i\omega_f) + NLF(y_f(i\omega)) \tag{6}$$

where $NLF(y_f(i\omega))$ is the first Fourier coefficient of the nonlinear function that reflects the nonlinear effects. This means that the solution is equal to the one obtained by a first-order HB, which ignores the nonlinear effects between different frequencies and the steady bias, and is still assumed adequate. As done for linear PFM, the loop is never closed and *NLF* is needed only for calculating the flutter gain, which is a non-iterative step. Since the response is now nonlinear, it depends on the excitation signal so that the modified *PFM* becomes

$$PFM\left(\omega_{pco}\right) = -20\log_{10}\left(\frac{P_f y_f\left(i\omega_{pco}\right) + NLF\left(y_f\left(i\omega_{pco}\right)\right)}{u_f\left(i\omega_{pco}\right)}\right)[dB] \tag{7}$$

where ω_{pco} is the cross-over frequency, i.e.

$$\Phi\left(\omega_{pco}\right) = \angle\left(\frac{P_f y_f\left(i\omega_{pco}\right) + NLF\left(y_f\left(i\omega_{pco}\right)\right)}{u_f\left(i\omega_{pco}\right)}\right) = 360^o n \tag{8}$$

The nonlinear term in Eqs. (6) thru (8) is first calculated over the frequency range of interest. At each frequency, the TD output is obtained by

$$y_f\left(t_j\right) = \mathrm{Re}\left(y_f\left(i\omega\right)e^{i\omega t_j}\right) \tag{9}$$

and serves as the only input to the SISO nonlinear block, which can be compounded by several nonlinear elements. The output $NLF(y_f(t))$ is transformed to FD by

$$NLF\left(y_f\left(i\omega\right)\right) = \frac{2}{N - Lk_0}\sum_{j=mk_0}^{N-1} NLF\left(y_f\left(t\right)\right)_j e^{-i\omega t_j} \tag{10}$$

where the number of time steps is $N=Lk$, L and k are the number of computation points per cycle and the number of cycles considered. The summation in Eq. (10) is performed with $NLF(y_f(t))$ after removing the initial k_0 cycles to avoid transient effects that might exists in the nonlinear function. The resulting $NLF(y_f(i\omega))$ is used to calculate the Bode plots associated with the right-hand side of Eq. (6), from which the cross-over frequencies of Eq. (8) are found, followed by the associated gains of Eq. (7). As done above for linear flutter, LCO occurs when $PFM(\omega_{pco}) = 0$dB. Since it now depends on the excitation amplitude, the process may be repeated with different excitations $u_f(i\omega)$, which yields the particular vibration level associated with LCO at each flight point.

2.3 Selection of the flutter parameter

As described and formulated above, the flutter parameter P_f should be one that expands the flutter velocity boundaries, and that its effect can be removed by a SISO control loop. Basic understanding of the flutter phenomena should normally be sufficient for selecting an adequate parameter. The selection of a parameter that does not increase the flutter velocity as desired would yield large response that is easy to detect. An example of a parameter that would work in most wing-flutter cases is an incremental generalized damping coefficient of the first-bending (i^{th}) mode, $P_f = \Delta g_i \, M_{hh,ii} \, \omega_i$ where Δg_i is the incremental non-dimensional coefficient, and $M_{hh,ii}$ and ω_i are the generalized mass and natural frequency of the i^{th} mode. Also, to obtain a significant effect, the magnitude of P_f may be much larger than typical values. The respective $[C_f(i\omega)]$ vector that defines y_f as a i^{th} modal velocity would be all zero except for $C_{f,i}=i\omega$ and the $\{B_f\}$ vector would be all zero except for $B_{f,i} = 1$, which applies the resulting generalized damping force.

Another example of an effective flutter parameter in typical bending-torsion or wing-store flutter mechanisms is an added mass, Δm, at the wing's tip leading edge. The input u_f and output y_f would be in this case a discrete force normal to the wing planform and the local acceleration to the same direction. The PFM equation of motion (2) would be applied in this case with $P_f = \Delta m$, $\{B_f\} = [\phi_y]^T$ and $[C_f(i\omega)]=-\omega^2[\phi_y]$, where $[\phi_y]$ is a row in the normal-mode matrix associated with the normal displacement at the added mass location. The flutter boundary of the original system is identified at the velocity and frequency where the applied force is equal, in magnitude and direction, to the measured acceleration times Δm. It implies that, physically, the harmonic excitation force is entirely dedicated to moving the added mass, while the rest of the aircraft retains its harmonic motion with no external excitation.

3 NUMERICAL EXAMPLES

This section is divided in two subsections. In the first, linear PFM flutter results obtained using the Dynresp code [10] are compared to those calculated using the *g* (ZAERO) and *p-k* (NASTRAN) methods. Two Generic Transport Aircraft (GTA) models are used. The first is with a simple gust-alleviation control system that exhibits a wing bending-torsion flutter mechanism, and the second, which is described in Ref. [9], has a softened horizontal tail plane (HTP) that exhibits bending-torsion flutter when the elevators are firmly connected through their actuators, and control-surface flutter when the actuators are disconnected. The aeroelastic models in both cases consist of normal modes extracted from a beam-type structural model with lumped masses, and an aerodynamic panel model as depicted in Fig. 1. In the second subsection, nonlinear-PFM LCO results are compared to direct time-marching simulations. In this case, we use the soften GTA with free play in the springs connecting the elevators to the HTP, as in [9].

3.1 Linear Example

The new PFM technique is applied to calculate the flutter characteristics of the two models discussed above. The GTA model with a gust-alleviation control system is used in Sec. 3.1.1, and the soften-HTP GTA model with and without the springs connecting the elevators to the HTP is used in Sec. 3.1.2.

3.1.1 GTA with gust-alleviation control system

The gust-alleviation control system is presented in Fig. 2, where "wing-tip acceleration" is the average accelerations measured at the right and left wing tips. Open- and closed-loop flutter

analyses were performed using symmetric modes only. The PFM results are compared to those obtained by the *g*-method implemented in ZAERO. The analyzed subcases are: (1) k_1=0 (open loop), (2) k_1=0.5, and (3) k_1=1.

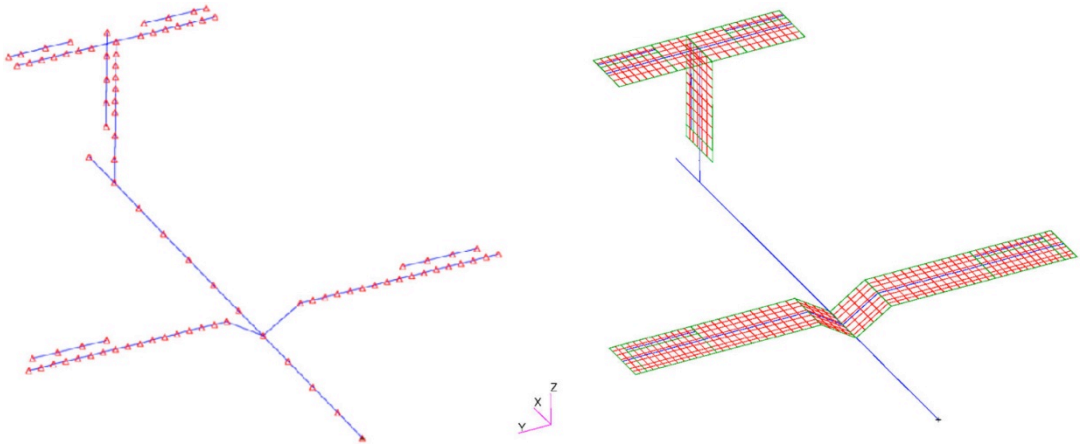

Figure 1: GTA Structural (left) and aerodynamic (right) model, taken from [9].

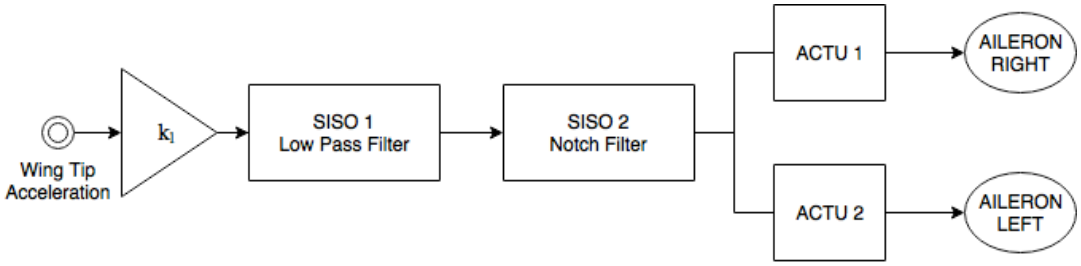

Figure 2: GTA gust-alleviation control system.

PFM stability analysis was first performed with the incremental modal damping Δg = 0.1 added to the first wing-bending mode, which is the third mode. With the generalized mass of $M_{hh,33}$=1.0 and the natural frequency of ω_3 = 50.0rad/s, the stabilizing parameter is P_f = 5.0. The PFM sensor, y_f, corresponds to the modal velocity, i.e. $y_f = i\omega\xi_3$, and the excitation corresponds to a generalized force at the same mode. As shown in Eq. (2), the effect of the stabilizing parameter is added to the system matrix while the feedback loop is disconnected in the response analysis.

The extraction of the flutter velocity and frequency in PFM is illustrated in Figs. 3, 4 and 5 using Subcase (1). Figure 3 shows the gain and phase associated with the FRFs of $P_f y_f(i\omega)$ in response to unit-amplitude u_f at V=161, 163 and 165m/s. The interpolated frequencies at which ϕ=0deg are the phase-cross-over frequencies ω_{pco}. These frequencies and the associated flutter margins of Eq. (5b), PFM=-$Gain(\omega_{pco})$, are plotted vs. velocity in Fig. 4 together with those of V=162 and 164m/s. The interpolated velocity at which PFM=0dB corresponds to V_f and the respective interpolated ω_{pco} is ω_f.

The PFM flutter velocities and frequencies are compared in Table 1 to those of ZAERO, exhibiting negligible differences attributed to different interpolation schemes. Table 2 presents the Subcase (3) flutter modes obtained with PFM and the *g*-method, also exhibiting excellent agreement. It may be noticed that the third mode is indeed a major participant in the flutter mechanism, but not necessarily the largest one.

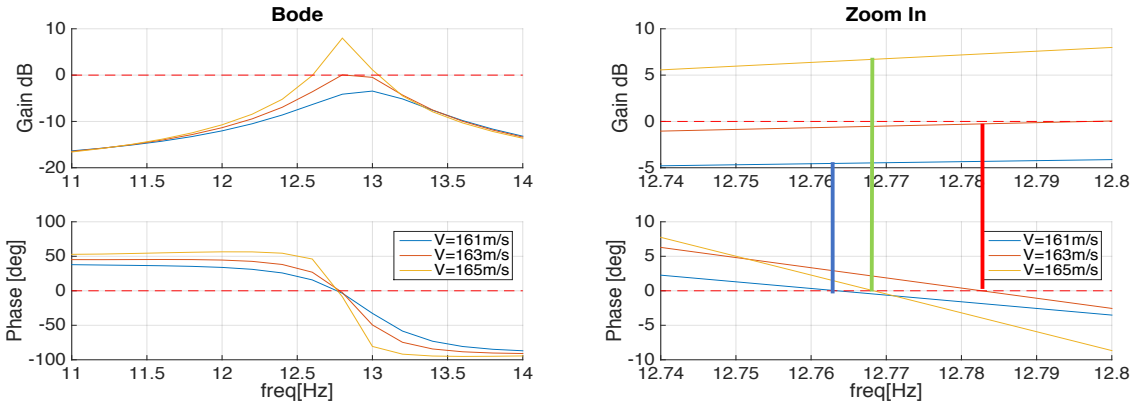

Figure 3: Bode Plots of $P_f y_f(i\omega)$ in Subcase (1).

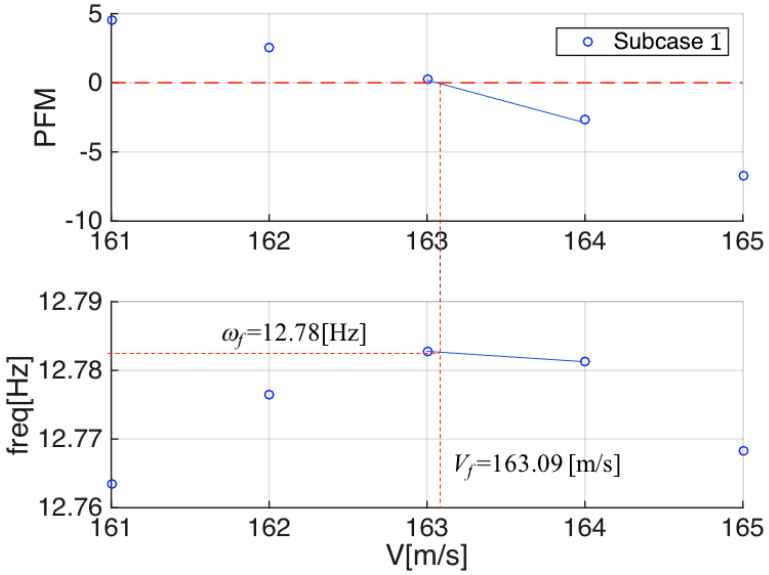

Figure 4: Bode Plots of $P_f y_f(i\omega)$ in Subcase (1).

	Subcase (1)		Subcase (2)		Subcase (3)	
	PFM	g	PFM	g	PFM	g
V_f [m/s]	163.09	163.18	153.12	153.13	143.62	143.8
Diff [%]	0.06	-	0.006	-	0.13	-
ω_f [Hz]	12.78	12.81	14.22	14.25	15.3	15.36
Diff [%]	0.23	-	0.21	-	0.39	-

Table 1: Comparison between PFM and *g*- methods.

Mode #	PFM		g		Mode #	PFM		g	
	Real	Imag	Real	Imag		Real	Imag	Real	Imag
1	-0.1514	-0.1203	-0.1520	-0.1199	6	-0.2539	0.0107	-0.2517	0.0089
2	0.0046	0.0120	0.0047	0.0120	7	0.0639	-0.0068	0.0628	-0.0068
3	0.5057	0.5650	0.5165	0.5555	8	-0.0018	-0.0081	-0.0020	-0.0081
4	-0.0161	-0.0015	-0.0161	-0.0015	9	-0.0278	-0.0218	-0.0279	-0.0219
5	1.0000	0.0000	1.0000	0.0000	10	-0.0056	0.0020	-0.0055	0.0020

Table 2: PFM and *g*- methods flutter modes for Subcase (3).

One of the advantages of the PFM method is that it utilizes efficient sensitivity analyses with respect to the stabilizing parameter P_f. To demonstrate this feature, the flutter calculations of

Subcases (2) and (3) were repeated with the control gain serving as $P_f = k_1 = 1.0$. Consequently, the stabilized system is the open-loop one (with $k_1 = 0$) and the FRFs are calculated from the input of SISO 1 in Fig. 2 to the wing-tip acceleration sensor. At each air velocity, ω_{pco} and $PFM = -G(\omega_{pco})$ are calculated as earlier, yielding in this case the classic Nyquist SISO gain margin (GM). The left plot in Fig. 5 shows the Bode plots for seven different velocities, and the blue circles in the right one show the variation of the GM and phase-cross-over frequencies with velocity. The GM=0dB point with k_1=1 in the GM plot is at V_f = 143.7m/s, agreeing with the one shown in Table 1. Flutter sensitivity analysis with respect to P_f can be easily performed by assuming, for example, P_f =0.5 instead of 1.0 without repeating the response simulations. This implies that k_1=0.5 is now a part of the original system, as in Subcase (2), while the other half of the original k_1 is the stabilizing element. This causes the GM plot in the right side of Fig. 5 to simply be shifted up by $20\log_{10}(2) \approx 6$dB, with no change in the frequency plot, leading to a new flutter point of (V_f =152.91m/s; ω_f =14.27Hz), which agrees with the one shown in Table 1.

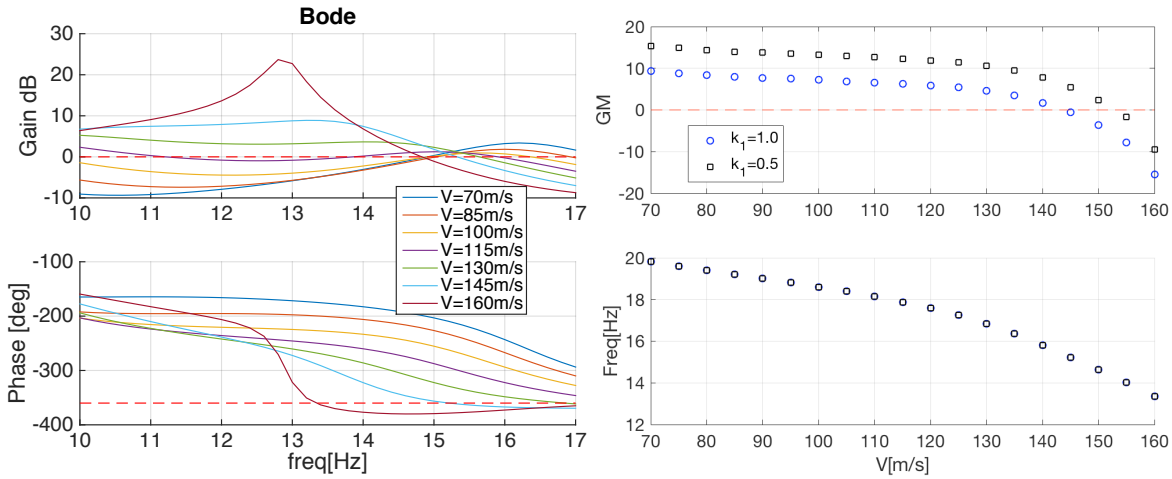

Figure 5: Left: Open-Closed Bode plots for k_1=1.0. Right: GM and phase-cross over frequencies for k_1=1.0 and 0.5, Subcases (2) and (3).

3.1.2 Control surface flutter

In this sub-subsection, linear flutter analyses of the soften-HTP GTA model in which the stiffness of the elevator actuators is represented by torsional springs, are presented. Two reference flutter cases, with connected and disconnected actuators, were analyzed using the common *p-k* method implemented in MSC/NASTRAN using two different sets of vibration modes. These cases were then analyzed using PFM with the spring condition modeled by a dummy control feedback loop that senses the rotation of the elevator relative to the HTP, multiplies it by the spring stiffness k_a and applies the resulting moment to the elevators about their hinges. This allows the two flutter cases to be modeled with one set of modes with the connected case analyzed with $k_a = -2\times10^4$ Nm/rad, that adds the nominal actuator spring, and the disconnected case with k_a=0Nm/rad. It should be noted that this model does not have any real control system. To obtain accurate results in the two flutter analyses, and in the nonlinear analyses of the next subsection, the single set of modes is generated with the elevator rotation degree of freedom loaded with a large fictitious inertia, as detailed in Refs. [9, 18], which is removed in the response analyses.

The PFM flutter analyses were repeated with two different stabilizing parameters P_f: (a) added generalized damping to the HTP first-bending mode; and (b) elevator actuator stiffness

coefficient of 4×10^4Nm/rad, which is twice the value of the nominal coefficient. The PFM results are shown in Table 3 in comparison with those obtained with the *p-k* method implemented in MSC/NASTRAN, exhibiting excellent agreement between PFM and *p-k*, and between the two selected PFM stabilizing parameters.

Actuator	Connected (C)– PFM		Disconnected (D) - PFM		C- *p-k*	D- *p-k*
P_f	Damping	Stiffness	Damping	Stiffness	-	-
V_f [m/s]	163.93	163.50	90.69	90.84	162.85	91.06
Diff [%]	0.66	0.40	0.41	0.24	-	-
ω_f[Hz]	12.71	12.70	12.19	12.19	12.7	12.19
Diff [%]	0.06	0.03	0.03	0.03	-	-

Table 3: PFM flutter results compared to *p-k*.

3.2 Nonlinear Example

In this subsection, we will show nonlinear results of the soften-HTP GTA, where the nonlinearity consists of rotational free play in the control-surface linkage to the HTP, while the actuators are locked. The structure is represented by the same modal basis used in Sec. 3.1.2.

The stabilizing element is a relatively stiff actuator spring (as in Sec. 3.1.2, $P_f=4\times10^4$Nm/rad) connecting the elevator to the HTP, while the original system is with disconnected actuators. The free-play nonlinear effects are introduced by a nonlinear SISO block that its input, y_f, is the rotation of the elevator relative to the HTP and its output, u_f, is the spring nonlinear moment, represented by the term $NLF(y_f)$ in Eq. (6). It is utilized in Dynresp by a dead-zone element multiplied by $-k_{a,nominal}=-2\times10^4$Nm/rad and its free-play limits are $\delta=\pm0.02$rad. To obtain a linear response with disconnected actuator, the PFM analysis was first performed with $u_f(i\omega)= P_f\delta=800$Nm that produces an elevator rotation amplitude of 0.02rad, which keeps the actuator disconnected by the nonlinear feedback block.

A discussed in Ref. [17], this model does not exhibit subcritical LCO and it is governed by the same mechanism in the entire LCO-velocity range between the disconnected and connected linear flutter velocities (91m/s<*V*<164m/s). Consequently, the first-order HB method discussed in this paper provides reasonably good results over the entire LCO range. Figure 6 shows the variation with velocity of the resulting LCO amplitude, divided by the free-play amplitude, and the fundamental LCO frequency, in comparison with comparison with direct time-domain simulations [9], both performed by Dynresp. It can be observed that the results agree fairly well.

The PFM results were obtained using a frequency window of [12,13]Hz in steps of 0.2Hz, with the *NLF* time history calculated for two response periods with 100 points per cycle. The total time for calculating the responses at 13 velocities for 19 excitation amplitudes was 6.0sec, whereas the time-marching simulations required for obtaining the time-marching plots of Ref. [9] required 119sec, not including the post-processing time.

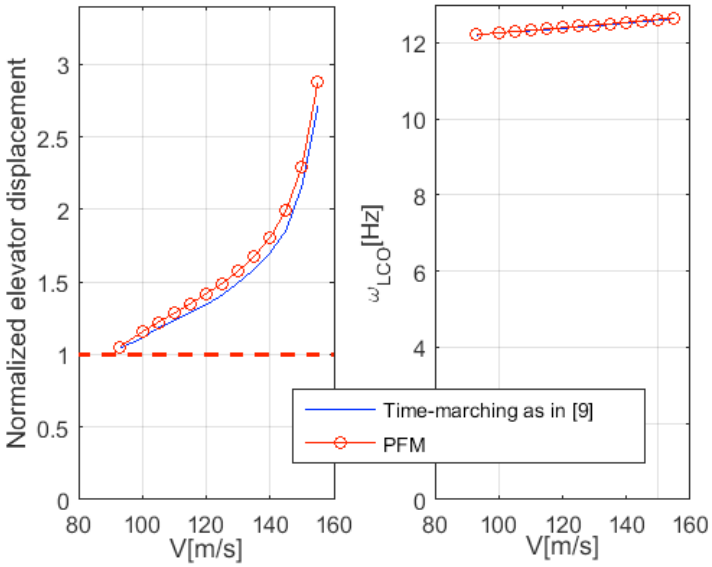

Figure 6: LCO Results.

4 CONCLUDING REMARKS

A new method for flutter analysis of aeroservoelastic systems, based on parametric flutter margins (PFMs), was presented. In contrast to standard flutter methods that extract the flutter onset conditions through the mathematical properties of the system matrix, the PFM method is based on response to harmonic excitation of the system to which a parameter that increases the flutter velocity beyond the search range is added. Flutter margins calculated with respect to the added parameter provide a numerically convenient environment for extracting the flutter velocity, frequency and mode of the original system in the searched range. The nonlinear PFM relies on the same principle as linear PFM, namely finding the conditions at which *PFM* = 0dB, based on Fourier transform of the response parameter at the excitation frequency. The linear flutter solution is obtained first and then used as a starting point. The main issue to be considered in the nonlinear PFM solution process is the way nonlinear effects are introduced. A new non-iterative approach equivalent to the first-order Harmonic Balance method was presented in this work.

Two Generic Transport Aircraft numerical models were used for proof of concept and validation of the new method. The linear PFM results are practically identical to those obtained using the common *p-k* (MSC/NASTRAN) and *g* (ZAERO) methods. The nonlinearities consisted of rotational free play in the control-surface actuators. As shown in the results sections, the LCO frequencies obtained by the PFM method agree with those obtained by the respective direct time-marching LCO solutions, while the amplitudes are up to 7% larger, which is acceptable for efficient design studies. The CPU time for obtaining the PFM results was about 20 times smaller than that of the time-marching approach.

With the PFM concept proved and simple-case results validated, the numerical process is still to be applied to more complex nonlinearity sources from different disciplines. It is already clear, however, that the new response-based parametric approach may be favorably used to obtain aeroelastic design sensitivities, investigation of nonlinear effects that might not be covered by ordinary flutter margins, integration with control design processes and interaction with describing-function and response-surface models. The technique developed can be

applied for flutter analysis using standard FD dynamic aeroelastic response codes such as MSC/NASTRAN, ZAERO or nonlinear response codes such as Dynresp.

5 REFERENCES

[1] Hassig, H. J., "An approximate true damping solution of the flutter equation by determinant iteration," *Journal of Aircraft*, Vol. 8, No. 11, 1971, pp. 885-889.

[2] Rodden, W. P., Harder, R. L., and Bellinger, E. D., "Aeroelastic Addition to NASTRAN," NASA CR 3094, 1979.

[3] Chen, P.C., "Damping perturbation method for flutter solution: the g-method." *AIAA Journal,* Vol. 38, No. 9, 2000, pp. 1519-1524.

[4] Karpel, M., Moulin, B., and Chen, P. C., "Extension of the g-method flutter solution to aeroservoelastic instability analysis," *Journal of Aircraft,* Vol. 42, No. 3, 2005, pp. 789-792.

[5] Roger, K. L., "Airplane math modeling methods for active control design," AGARD CP-228, Aug. 1977.

[6] Karpel, M., "Design for active flutter suppression and gust alleviation using state-space aeroelastic modeling," *Journal of Aircraft,* Vol. 19, No. 3, 1982, pp. 221-227.

[7] Conner, M., Tang, D., Dowell, E., and Virgin, L., "Nonlinear behavior of a typical airfoil section with control surface freeplay: a numerical and experimental study," *Journal of Fluids and Structures*, Vol. 11, No. 1, 1997, pp. 89–109.

[8] Chen, P, C. and Sulaeman, E., "Nonlinear response of aeroservoelastic systems using discrete state-space approach," *AIAA Journal*, Vol. 41, No. 9, 2003, pp. 1658–1666.

[9] Karpel, M., Shousterman, A., Maderuelo, C., and Climent, H., "Dynamic aeroservoelastic response with nonlinear structural elements," *AIAA Journal*, Vol. 53, No. 11, 2015, pp. 3233–3239.

[10] DYNRESP-11, Dynamic stability response of aircraft structures to gusts, maneuver commands and direct forces - Theoretical manual, Software Package, Ver. 11, KDC, 2017.

[11] Yang, Z. and Zhao, L., "Analysis of limit cycle flutter of an airfoil in incompressible flow," *Journal of Sound and Vibration*, Vol. 123, No. 1, 1988, pp. 1–13.

[12] Manetti, M., Quaranta, G., and Mantegazza, P., "Numerical evaluation of limit cycles of aeroelastic systems," *Journal of Aircraft*, Vol. 46, No. 5, 2009, pp. 1759–1769.

[13] Liu, L. and Dowell, E. H., "Harmonic balance approach for an airfoil with a freeplay control surface," *AIAA Journal*, Vol. 43, No. 4, 2005, pp. 802–815.

[14] Dimitriadis, G., "Continuation of higher-order harmonic balance solutions for nonlinear aeroelastic systems," *Journal of Aircraft*, Vol. 45, No. 2, 2008, pp. 523–537.

[15] Fichera, S. and Ricci, S., "Freeplay-induced limit-cycle oscillations in a T-tail: numerical vs experimental validation," *Journal of Aircraft*, Vol. 52, No. 2, 2014, pp. 486–495.

[16] Ogata, K., *Modern Control Engineering,* 4th ed., Prentice-Hall, Upper Saddle River, NJ, USA, 2002.

[17] Roizner, F. and Karpel, M., "Linear and Nonlinear Flutter Analyses Using Dynamic Response Computations," AIAA-2017-1594, presented at the Scitech Forum, Grapevine, TX, USA, January 2017.

[18] Karpel, M. and Raveh, D., "Fictitious mass element in structural dynamics," *AIAA Journal*, Vol. 34, No. 3, 1996, pp. 607-613.

COPYRIGHT STATEMENT